

Supporting Information

Ternary Molybdenum Sulfoselenide Based Hybrid Nanotubes Boosts Potassium-Ion Diffusion Kinetics for High Energy/Power Hybrid Capacitors

*Jingyu Gao,^{‡a} Gongrui Wang,^{‡a} Yi Liu,^a Jie Li,^a Bo Peng,^a Shuhong Jiao,^a Suyuan Zeng^{*b} and Genqiang Zhang^{*a}*

^aHefei National Laboratory for Physical Sciences at the Microscale, CAS Key Laboratory of Materials for Energy Conversion, Department of Materials Science and Engineering, University of Science and Technology of China, Hefei 230026, China

^bDepartment of Chemistry and Chemical Engineering, Liaocheng University, Liaocheng 252059, China

[‡]These authors contribute equally to this work.

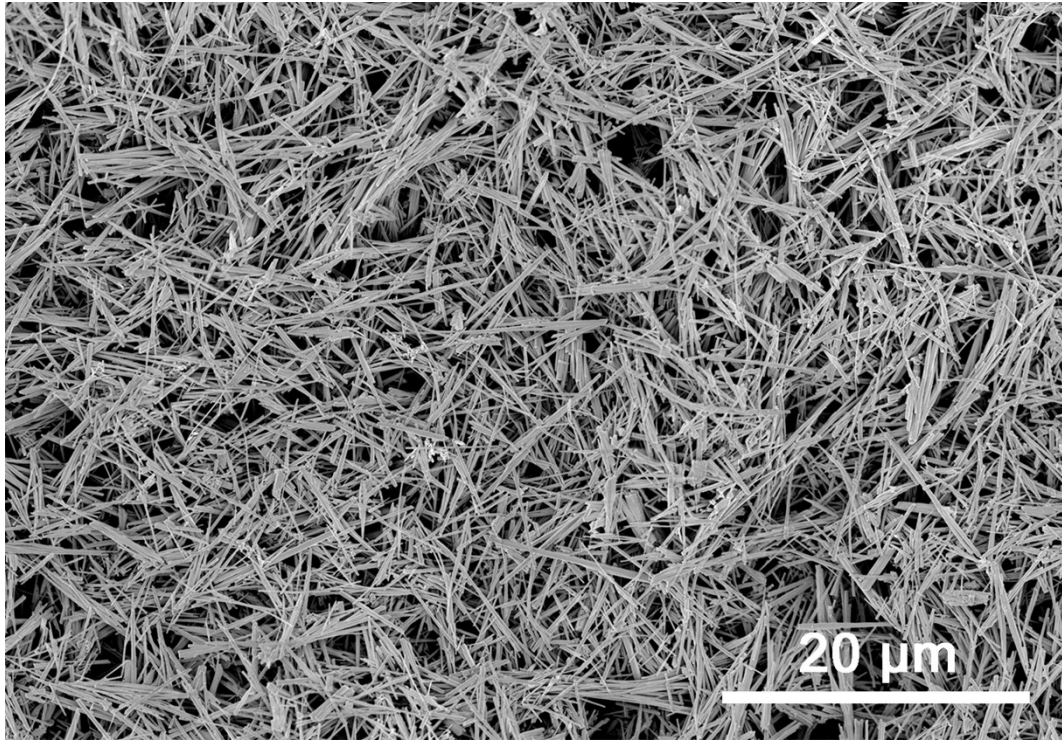


Figure S1. Low-magnification image of Sb₂S₃ nanowires.

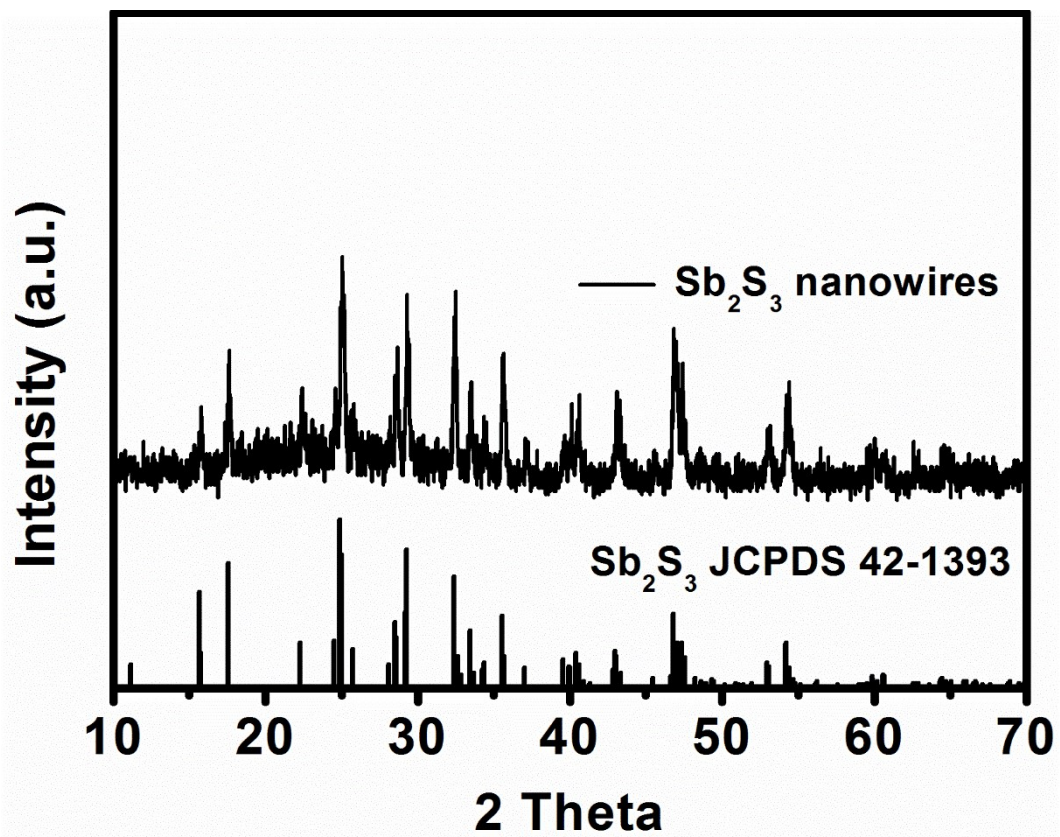


Figure S2. XRD pattern of Sb₂S₃ nanowires.

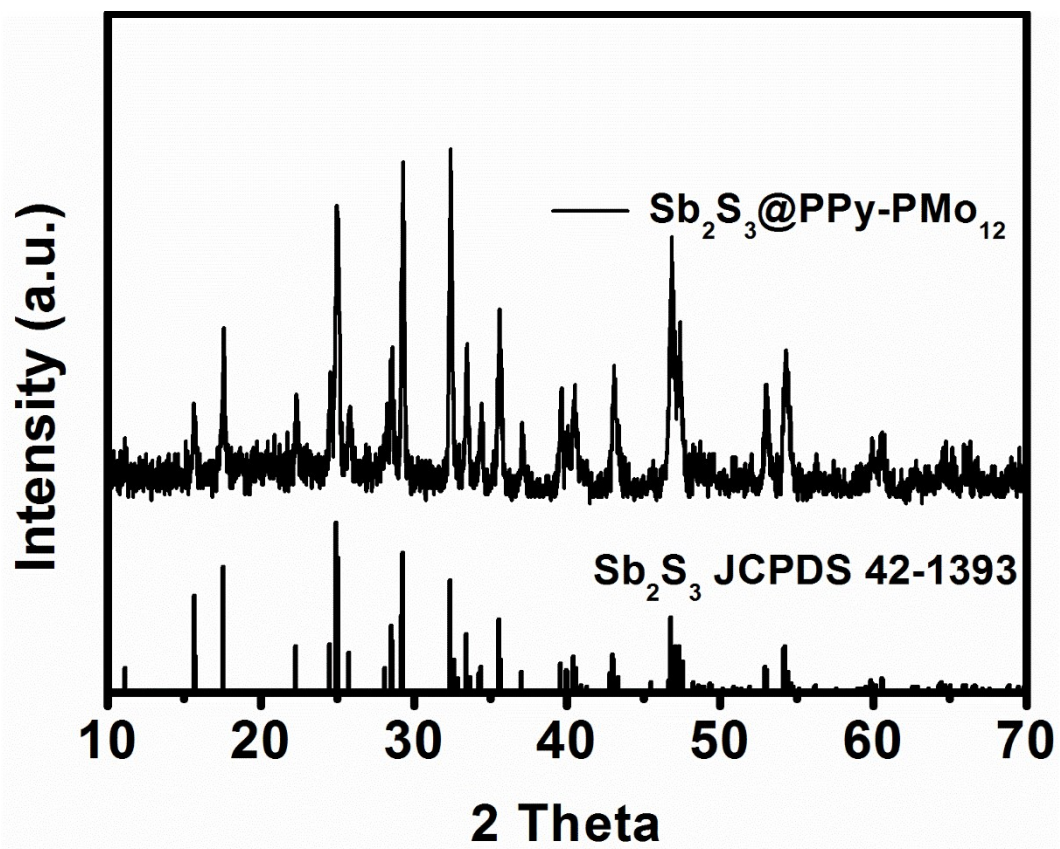


Figure S3. XRD pattern of $\text{Sb}_2\text{S}_3@PPy\text{-PMo}_{12}$ core-shell nanowires.

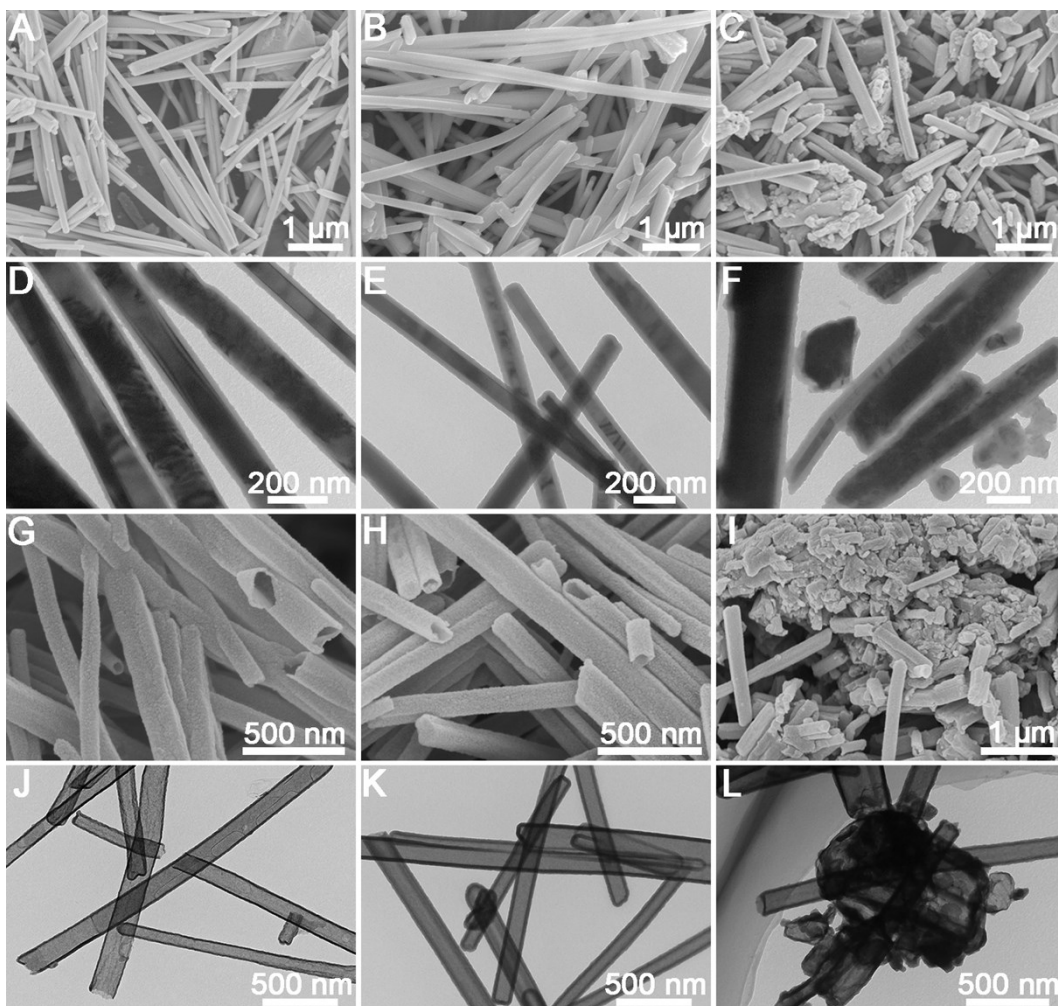


Figure S4. SEM and TEM images of $\text{Sb}_2\text{S}_3@\text{PPy-PMo}_{12-0.06}$ (A, D), 0.09 (B, E), 0.12 (C, F) core-shell nanowires and corresponding $\text{MoS}_2-0.06$ (G, J), 0.09 (H, K) and 0.12 (I, L) products after annealing treatment.

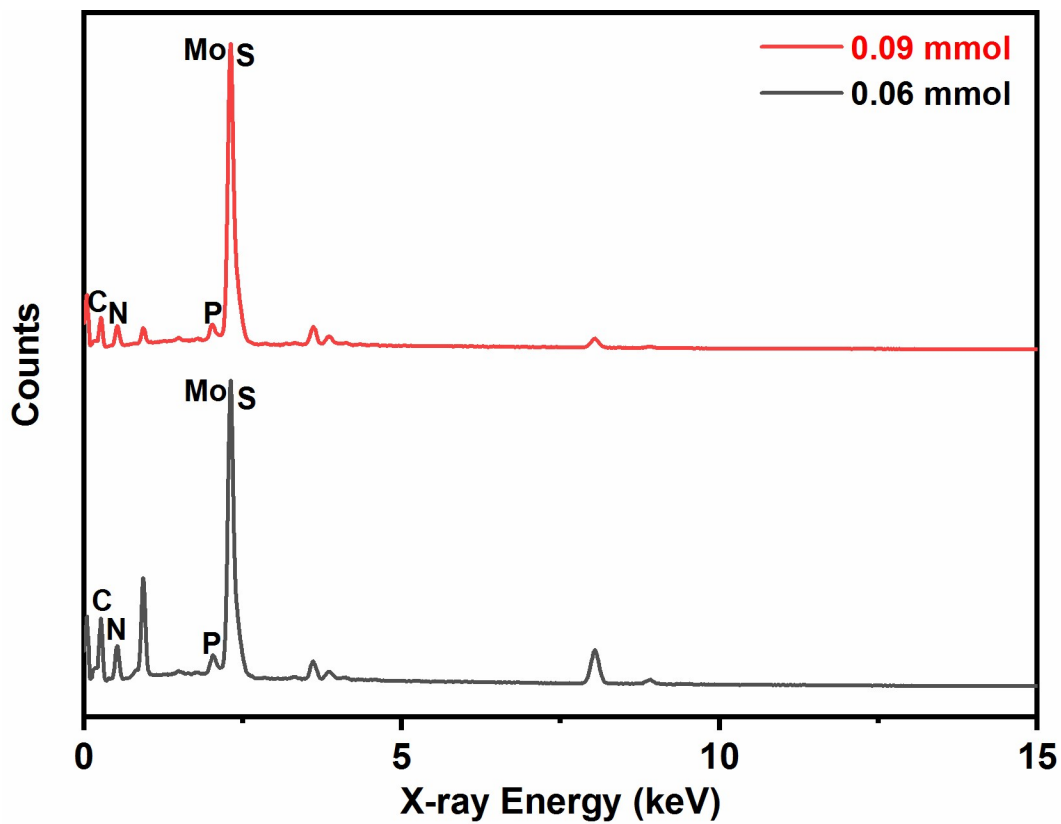


Figure S5. Energy dispersive X-ray spectroscopy (EDS) result of MoS₂-0.06 and 0.09 nanotubes.

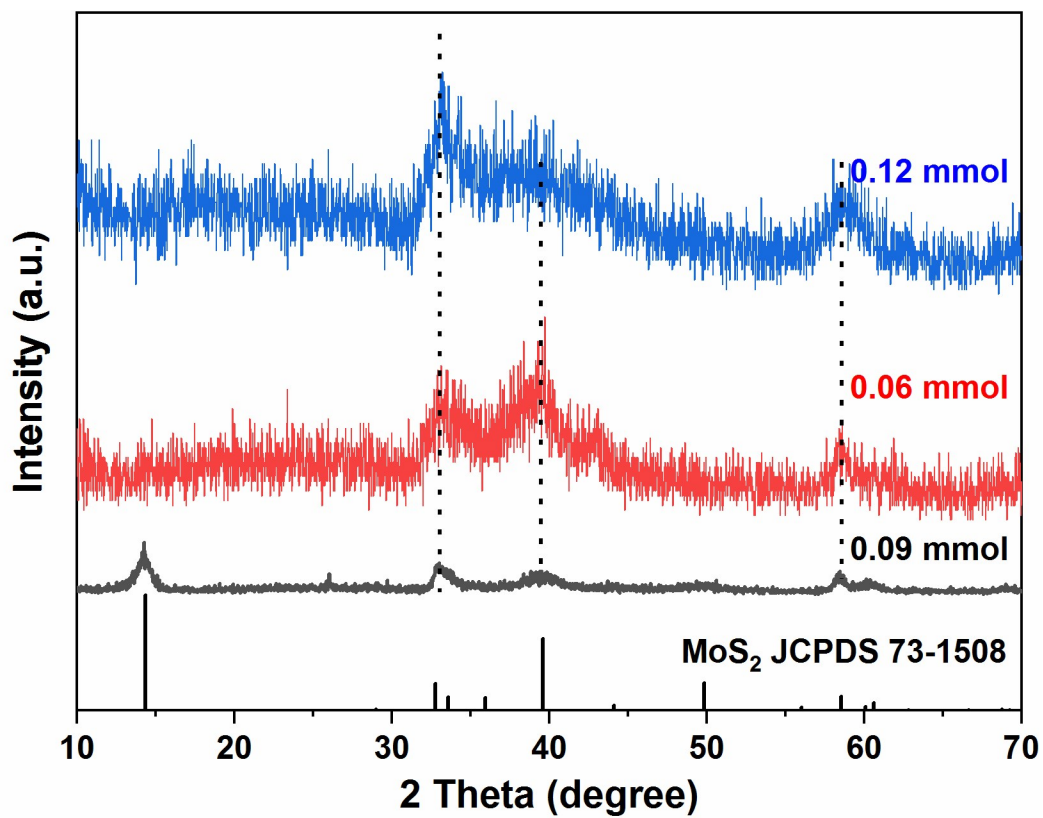


Figure S6. XRD patterns of MoS₂-0.06, 0.09 and 0.12 products.

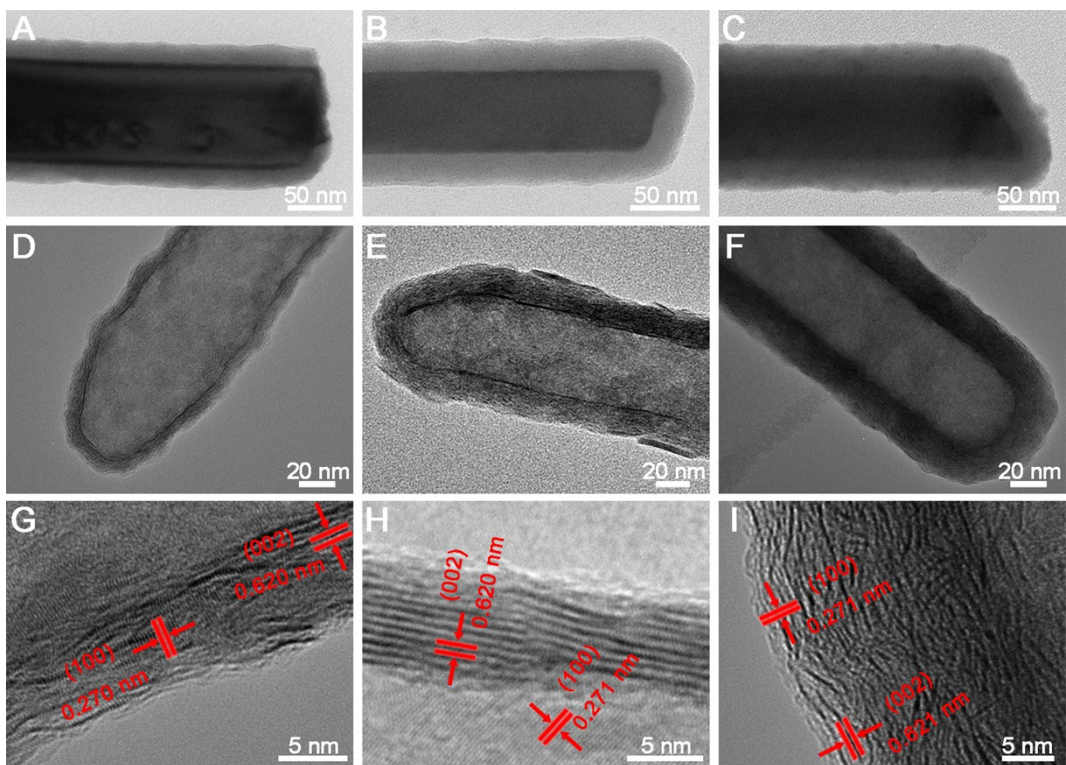


Figure S7. TEM images of (A, D) MoS₂-0.06, (B, E) 0.09 and (C, F) 0.12 nanotube before and after annealing treatment. Corresponding HRTEM analysis of MoS₂-0.06 (G), 0.09 (H) and 0.12 (I) nanotube.

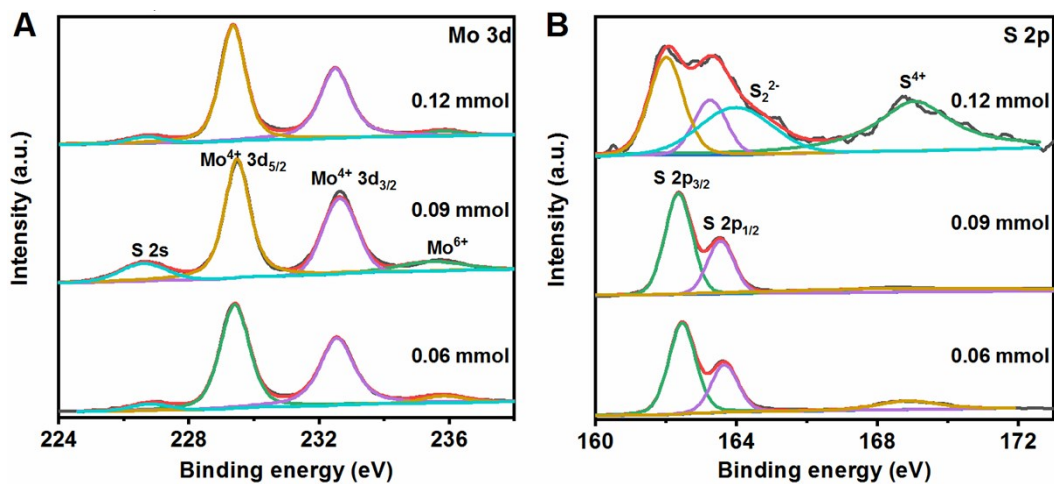


Figure S8. A) Mo 3d and B) S 2p XPS spectra of MoS₂-0.06, 0.09 and 0.12 nanotubes.

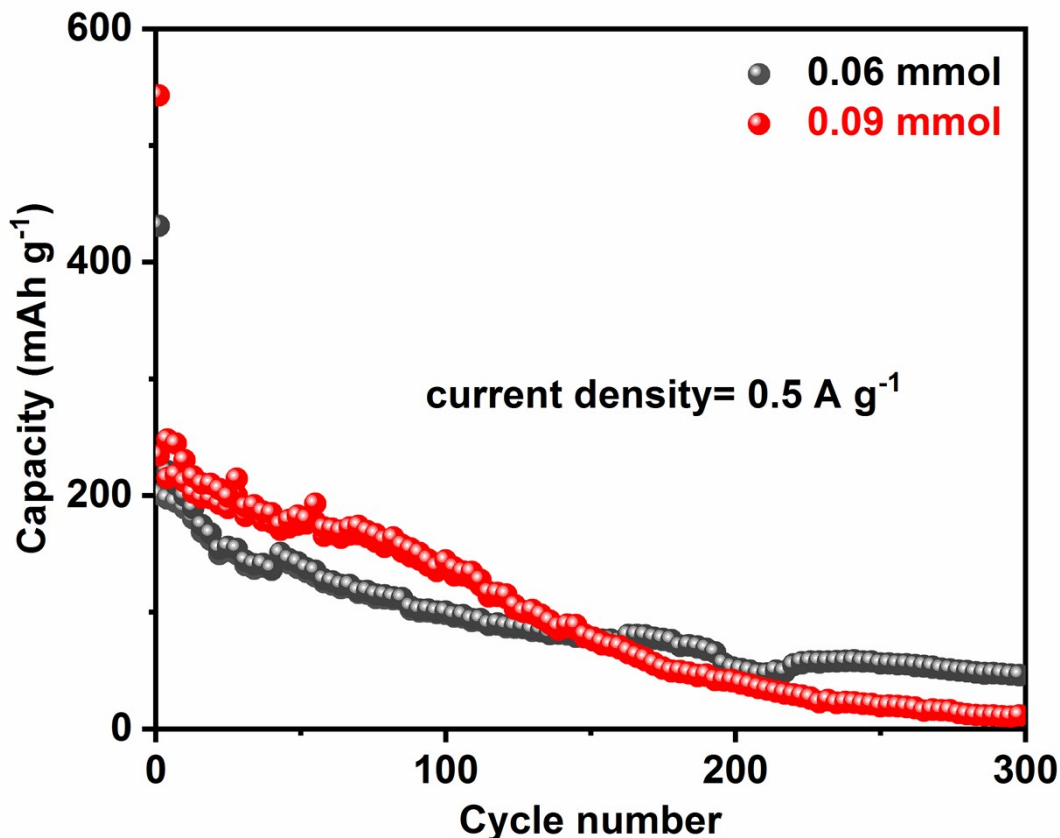


Figure S9. Cycling performance of MoS₂-0.06 and 0.09 samples at the current density of 0.5 A g⁻¹.

In regard to the effect of different wall thicknesses on the performance of MoS₂, we have carried out two comparative experiments, by just changing the added amounts of phosphomolybdic acid from original 0.09 mmol to 0.06 mmol and 0.12 mmol, respectively (denoted as MoS₂-0.06, MoS₂-0.09, MoS₂-0.12). As shown in **Fig. S4**, Sb₂S₃ templates still exhibit uniform nanowire morphology with smooth surface after coating with PPy-PMo₁₂ layer when the added amount of phosphomolybdic acid is 0.06 mmol and 0.09 mmol. Besides, the energy dispersive X-ray spectroscopy (EDS) result of MoS₂-0.06 and 0.09 nanotubes in **Fig. S5** indicate that the successful doping of N, P elements into the wall of MoS₂/C tubes with Mo/S molar ratio

about 1/2. However, with the amount of phosphomolybdic acid increased to 0.12 mmol, a great deal of impurities can be observed in SEM and TEM images after PPy-PMo₁₂ layer coating on the surface of Sb₂S₃ template, while big chunks of impurities still remain after annealed at high temperature, which is bound to result in awful cycling performance of MoS₂-0.12 compared to the uniform hollow nanotubes in MoS₂-0.06 and MoS₂-0.09 samples. Further, whether the added amount of phosphomolybdic acid increases or decreases, the main diffraction peaks of MoS₂-0.06, MoS₂-0.09 and MoS₂-0.12 product could still be indexed well to MoS₂ phase (JCPDS 73-1508) in **Fig. S6**. As shown in **Fig. S7**, hollow nanotubes with wall thickness about 15 nm (MoS₂-0.06) could be prepared after thermal annealing treatment, while the thickness of the wall composed of MoS₂ and C compared to that of MoS₂-0.09, is reduced partly. Impurities aside in MoS₂-0.12 product, the wall thickness of single nanotube still tend to be enlarged owing to the increased polymerization degree of pyrrole monomer initiated by the oxidizing PMo₁₂, while excessive MoS₂ layers are scattered in the thick wall consist of MoS₂ and C notably. In addition, the results of X-ray photoelectron spectroscopy (XPS) analysis manifest the similar chemical composition and surface electronic state of these three samples in **Fig. S8**. Finally, to explore the direct relation between wall thicknesses and cycling performance, MoS₂-0.06 and MoS₂-0.09 hollow nanotubes were used as anode materials to investigate electrochemical capability in PIBs (**Fig. S9**). When cycling at the current density of 0.5 A g⁻¹, the capacity of MoS₂-0.06 is much lower than that of MoS₂-0.09, which also reveals more instability. The reduction of phosphomolybdic acid in the preparation process of MoS₂ could obtain thinner wall of hollow nanotubes, such slight wall cannot tolerate large volume expansion during the insertion and exaction process of large potassium ions, leading to even

worse cycling performance. Given all that, suitable amount of phosphomolybdic acid in the process of polymerization could not only promote the purity of the coated product with uniform morphology, but provide proper wall thickness of final hollow tubes, ensuring relatively good performance compared with control samples, which is in accordance with the ratio of nine Py rings per PMo_{12} molecule to balance the charges during the polymerization process of a pyrrole (Py) monomer initiated by the oxidizing PMo_{12} (Adv. Mater., 1997, 9, 144). The followed comparison of characterization results and cycling properties between pure MoS_2 and $\text{MoS}_{2-x}\text{Se}_x/\text{C-HNTs}$ with different molar ratio of S/Se were based on 0.09 mmol amount of phosphomolybdic acid.

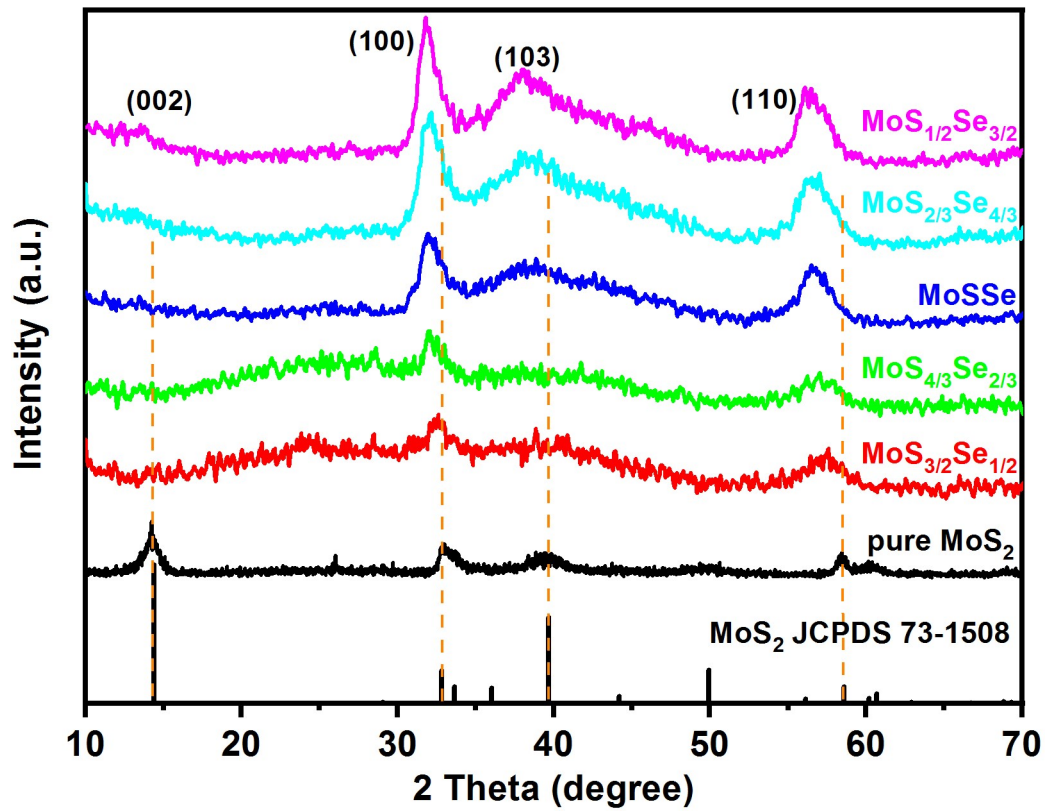


Figure S10. XRD patterns of pure MoS_2 and $\text{MoS}_{2-x}\text{Se}_x/\text{C-HNTs}$ with different molar ratio of S/Se.

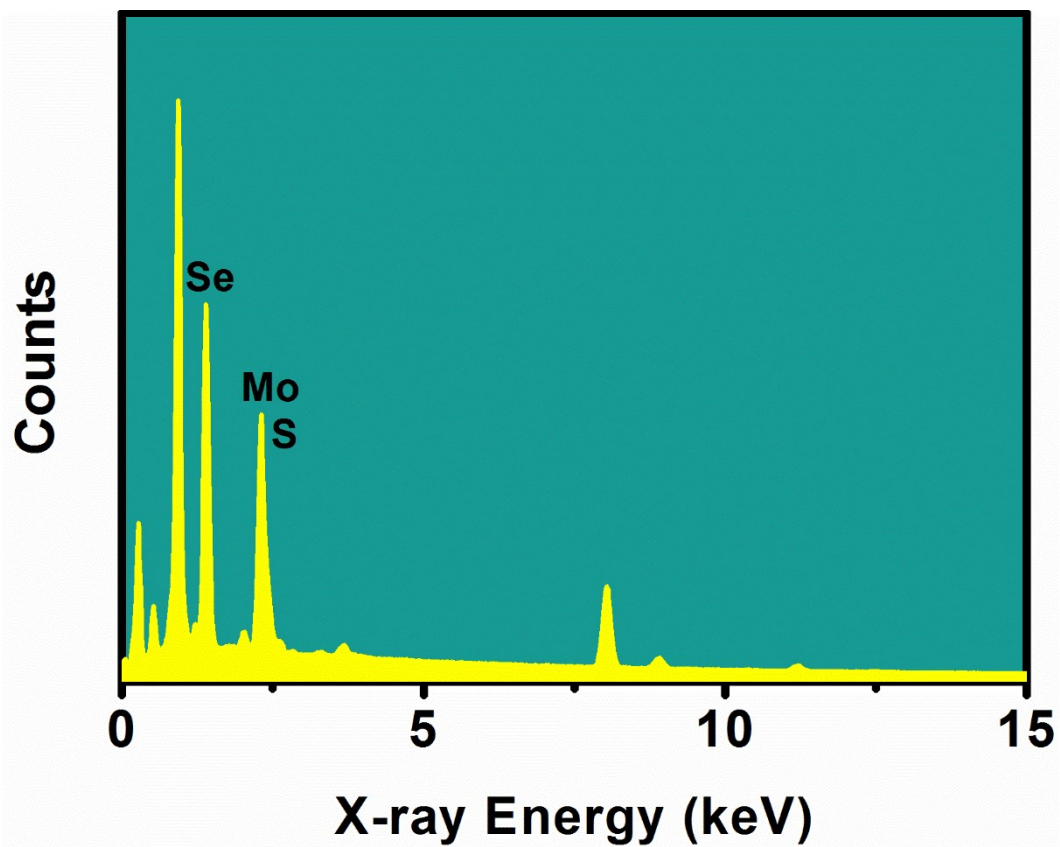


Figure S11. Energy dispersive X-ray spectroscopy (EDS) result of $\text{MoS}_{2/3}\text{Se}_{4/3}/\text{C-HNTs}$.

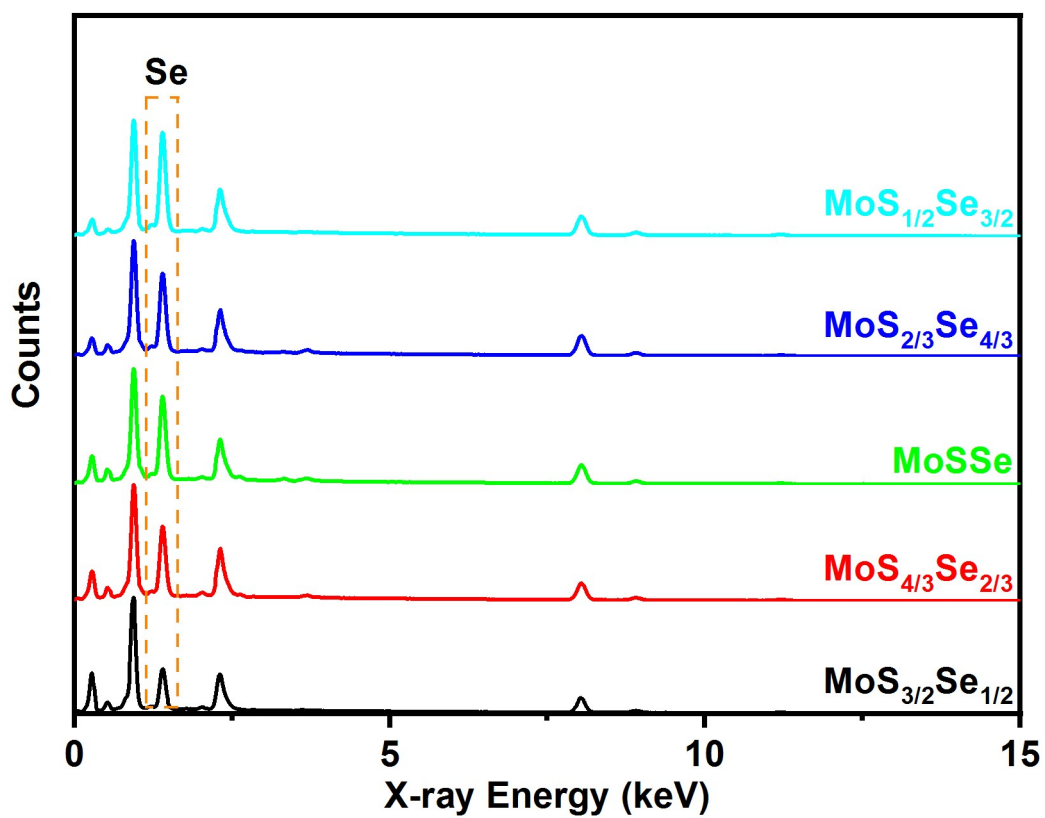


Figure S12. Energy dispersive X-ray spectroscopy (EDS) result of MoS_{3/2}Se_{1/2}, MoS_{4/3}Se_{2/3}, MoSSe, MoS_{2/3}Se_{4/3} and MoS_{1/2}Se_{3/2} nanotubes.

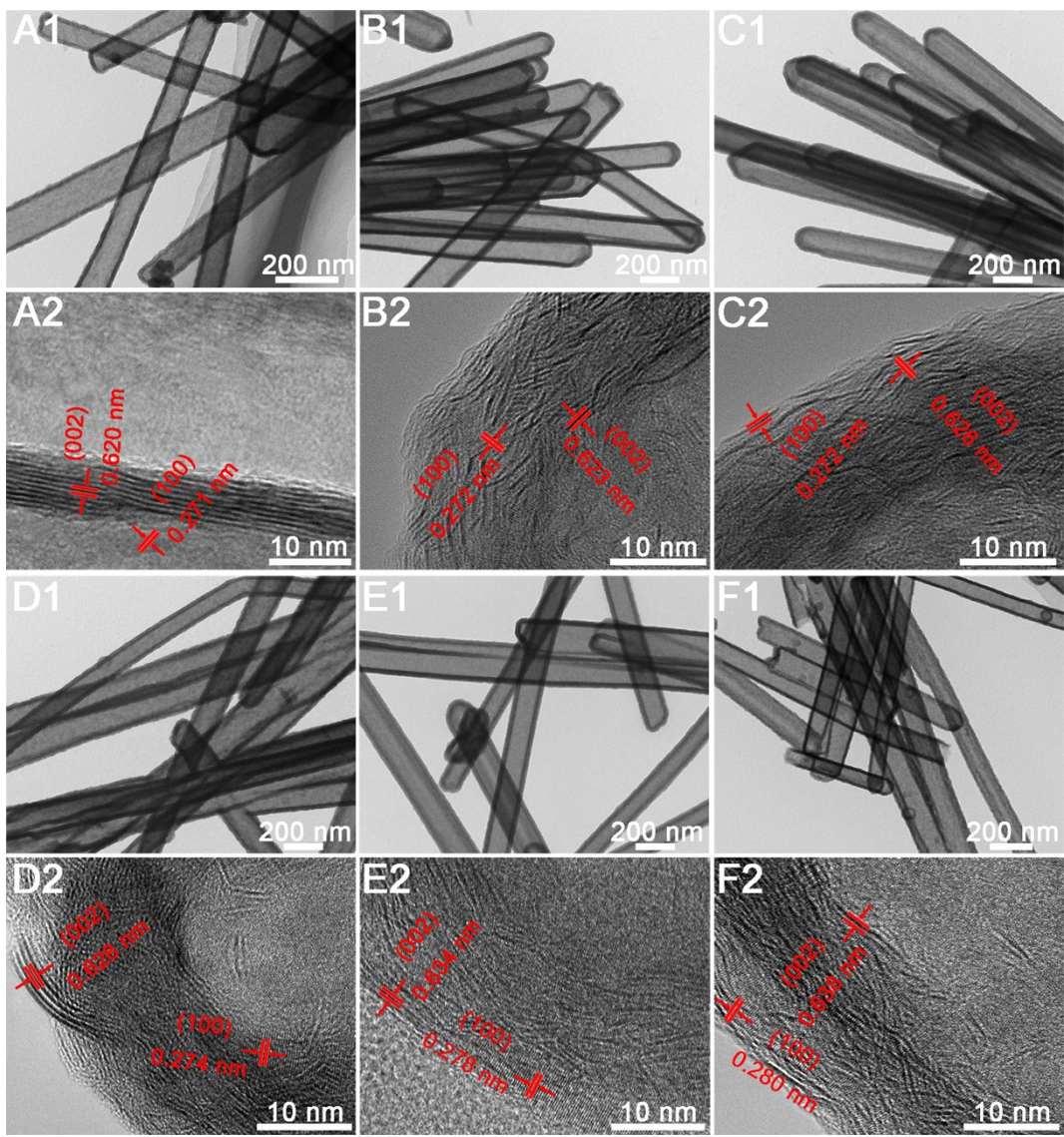


Figure S13. HRTEM analysis of pure MoS₂ (A1, A2), MoS_{3/2}Se_{1/2} (B1, B2), MoS_{4/3}Se_{2/3} (C1, C2), MoS_{Se} (D1, D2), MoS_{2/3}Se_{4/3} (E1, E2) and MoS_{1/2}Se_{3/2} nanotubes (F1, F2).

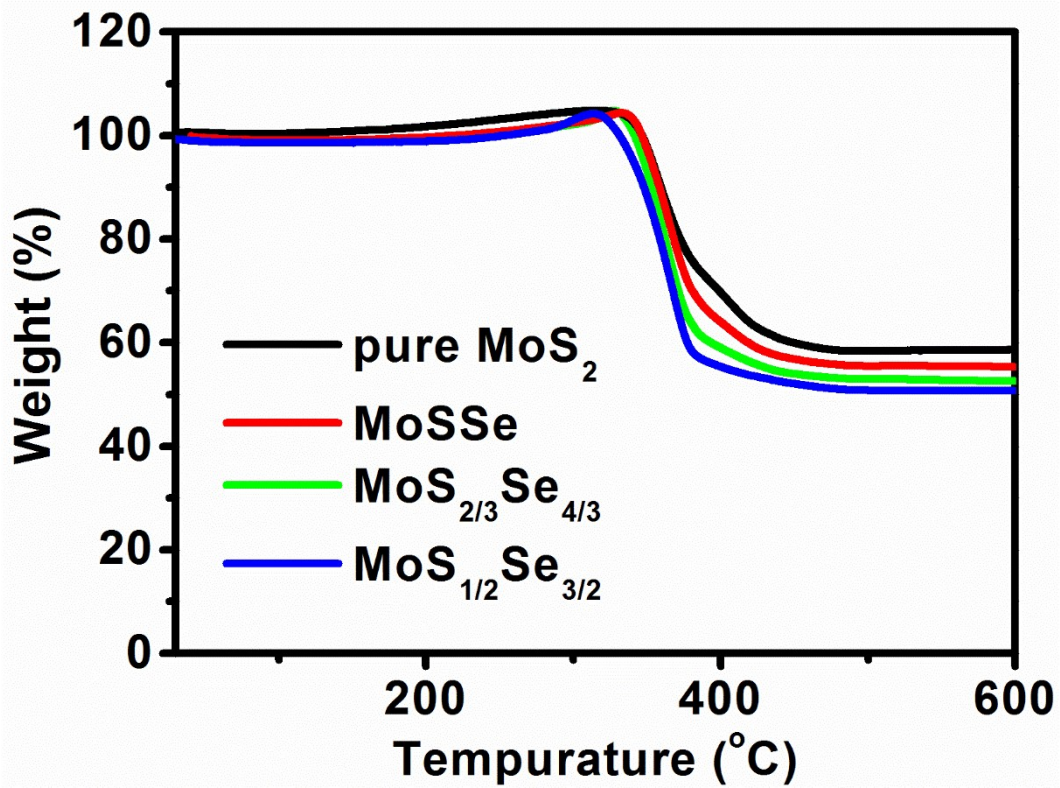


Figure S14. TG curves of pure MoS_2 and $\text{MoS}_{2-x}\text{Se}_x/\text{C-HNTs}$ with different molar ratio of S/Se.

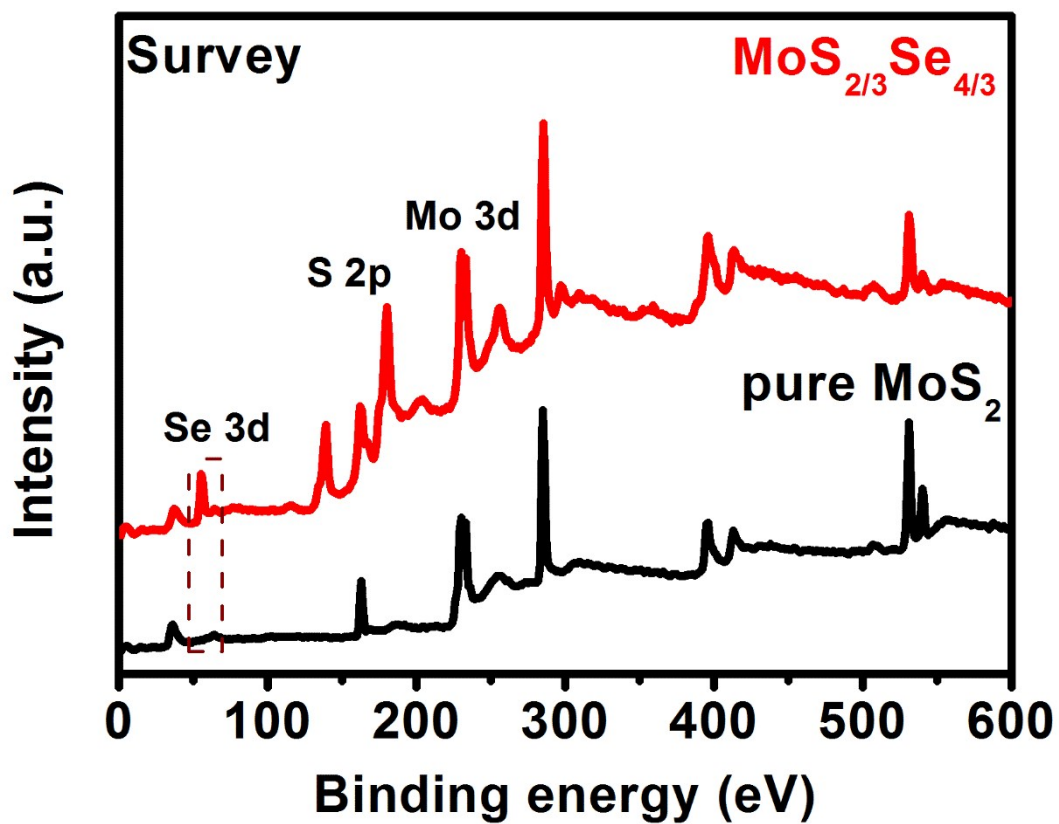


Figure S15. Survey spectrum of MoS_{2/3}Se_{4/3}/C-HNT and pure MoS₂.

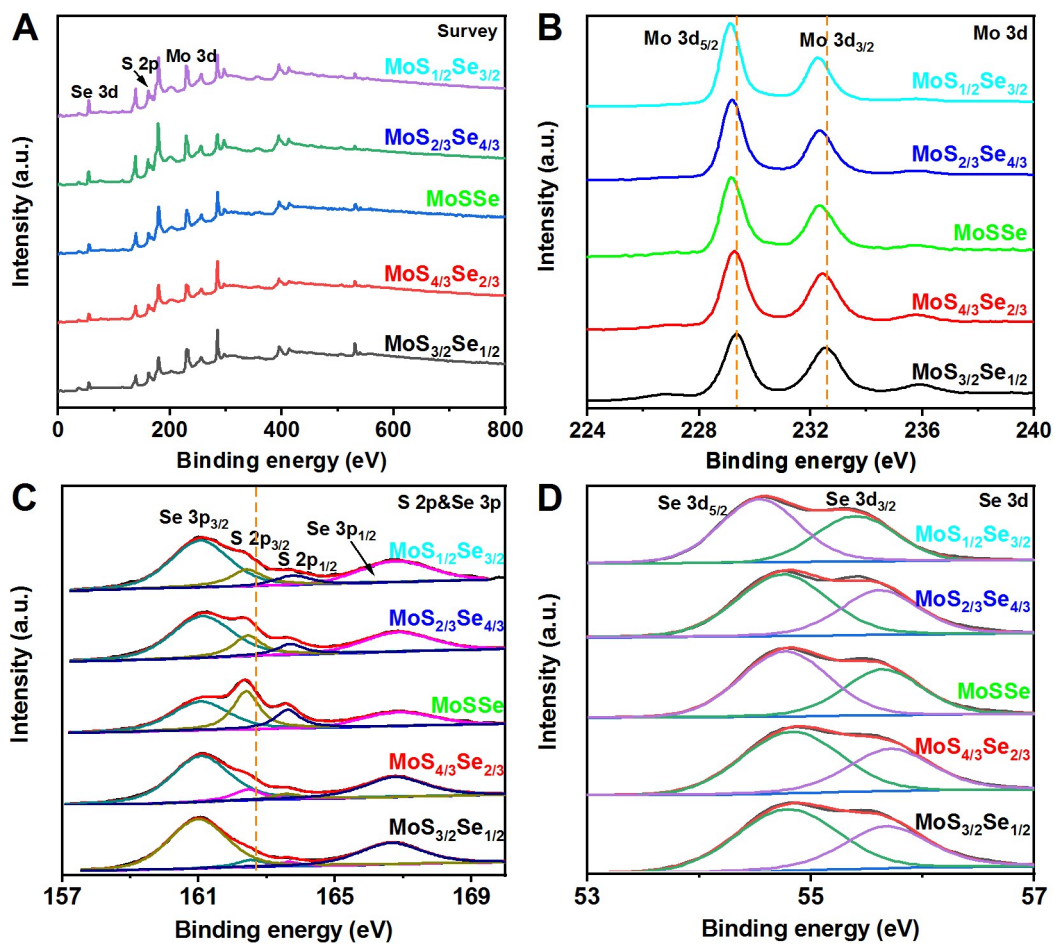


Figure S16. XPS spectra of MoS_{3/2}Se_{1/2}, MoS_{4/3}Se_{2/3}, MoSSe, MoS_{2/3}Se_{4/3} and MoS_{1/2}Se_{3/2} nanotubes.

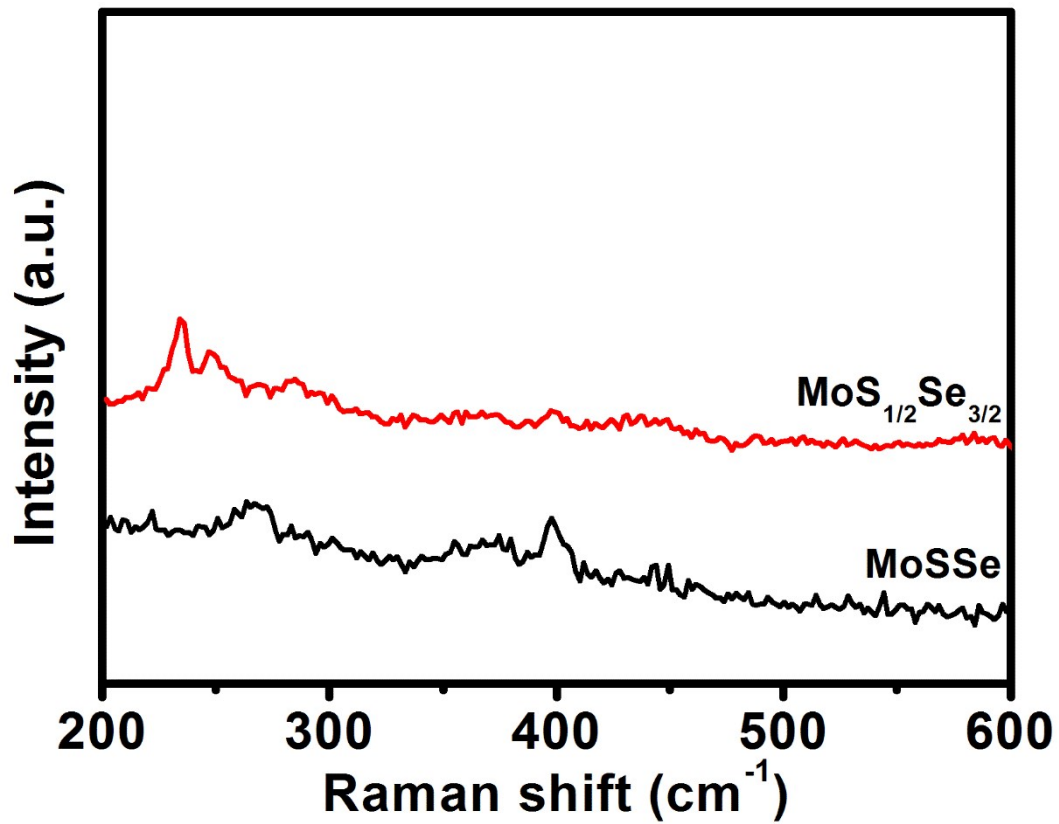


Figure S17. Raman spectra of MoSSe and MoS_{1/2}Se_{3/2} nanotubes.

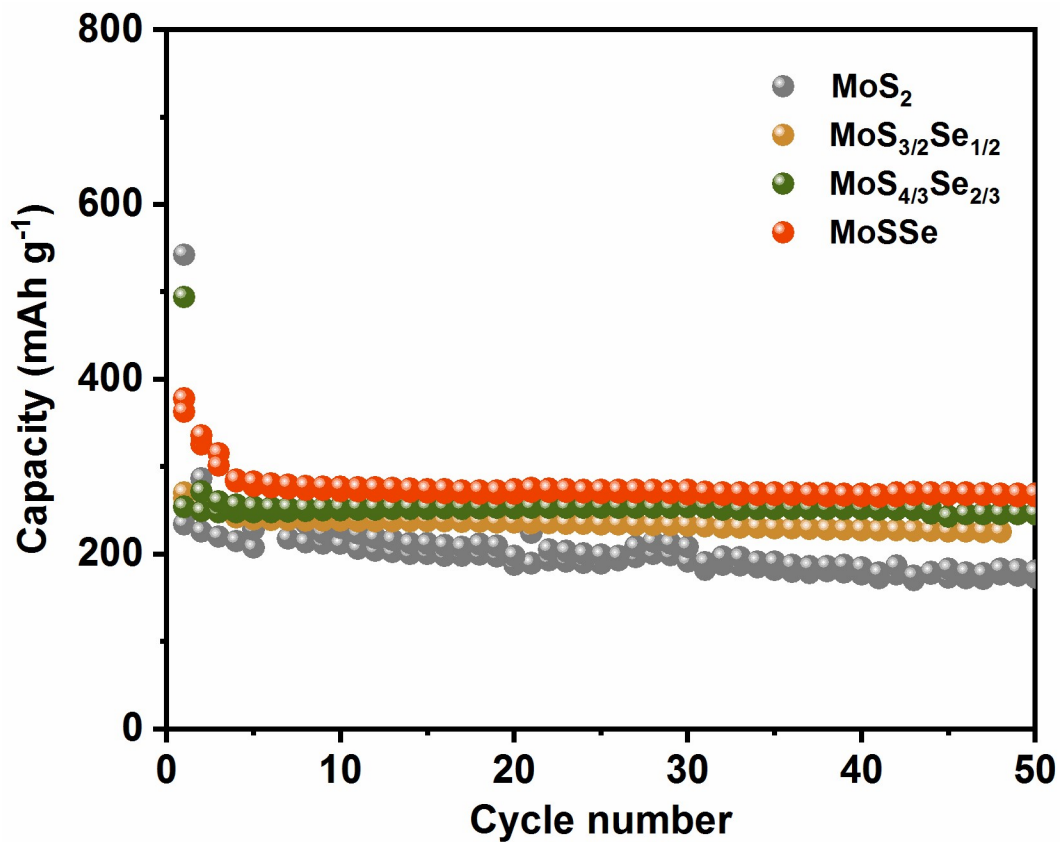


Figure S18. Comparison of cycling performance at 0.5 A g⁻¹ between MoS₂, MoS_{3/2}Se_{1/2}, MoS_{4/3}Se_{2/3} and MoSSe.

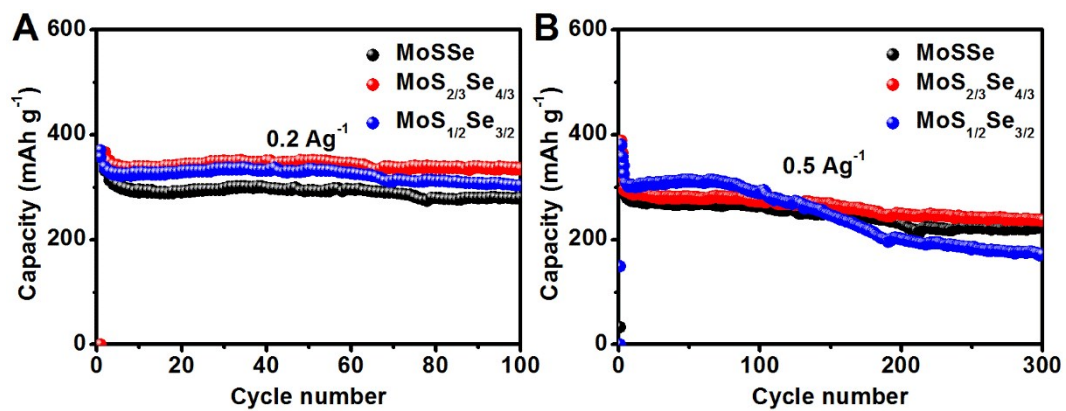


Figure S19. Cycling performance comparison of MoSSe, MoS_{2/3}Se_{4/3} and MoS_{1/2}Se_{3/2}/C HNT at current density of 0.2 A g⁻¹ and 0.5 A g⁻¹.

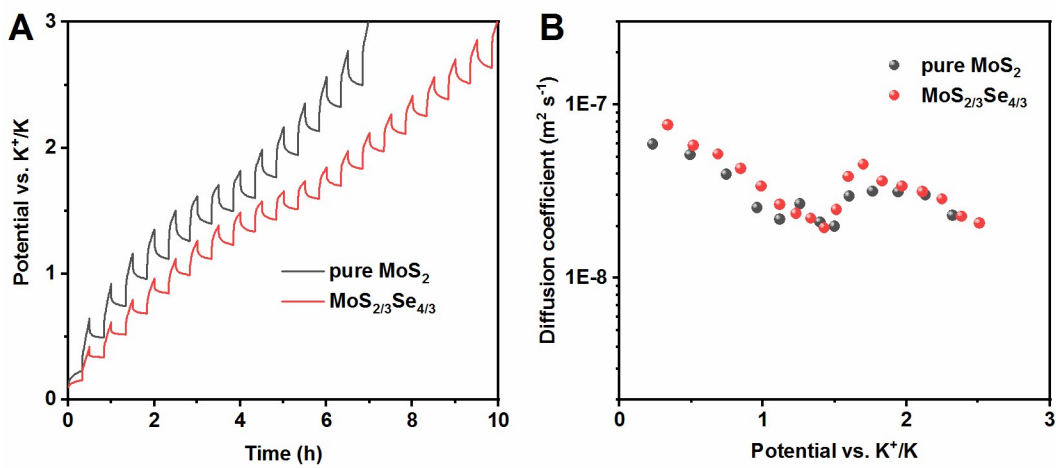


Figure S20. (A) GITT curves and (B) Corresponding K^+ diffusion coefficient of $MoS_{2/3}Se_{4/3}/C-HNT$ and MoS_2 electrode during the charge process.

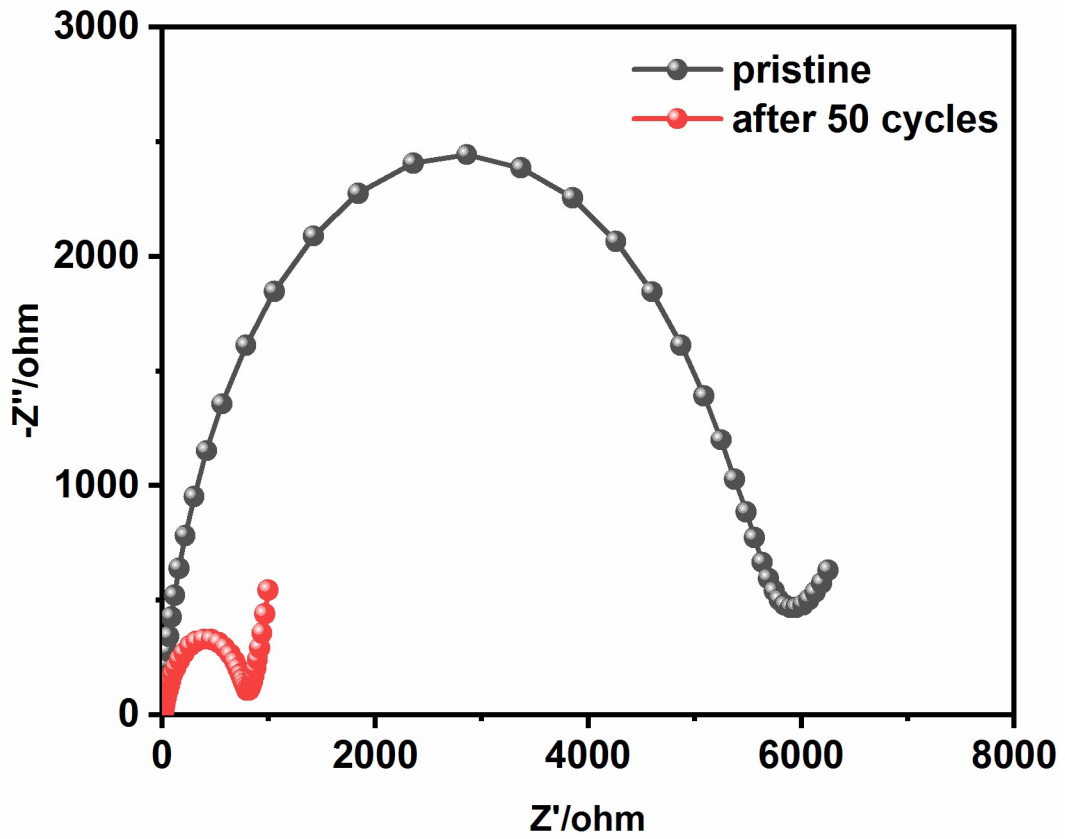


Figure S21. EIS spectra of MoS₂/3Se₄/3 after 50 cycles compared with pristine stage.

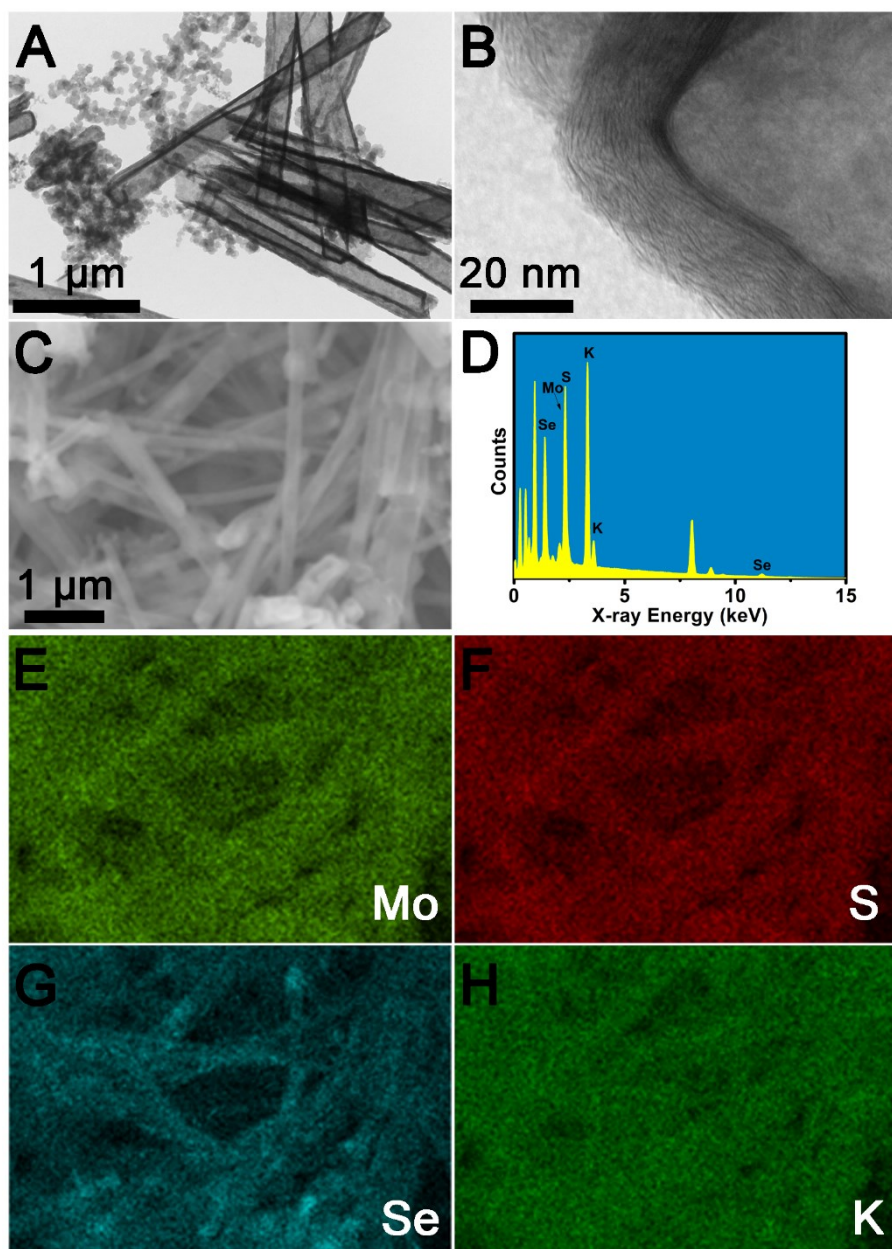


Figure S22. TEM (A, B) and SEM (C) of $\text{MoS}_{2/3}\text{Se}_{4/3}/\text{C}$ HNT anode after 100 cycles at 0.2 A g^{-1} ; Corresponding EDX result (D) and elemental mapping of Mo (E), S (F), Se (G) and K (H).

Table S1. Comparison of theoretical and experimental capacities between pure MoS₂ and MoS_{2-x}Se_x samples. Experimental values are discharge capacity of 10th cycle for each sample.

Samples	molar mass (g mol ⁻¹)	Theoretical capacity (mAh g ⁻¹)	Experimental value (mAh g ⁻¹)
MoS ₂	160.0	670.0	230.1
MoS _{3/2} Se _{1/2}	183.5	584.2	240.4
MoS _{4/3} Se _{2/3}	191.3	560.4	253.5
MoSSe	207.0	517.9	276.8
MoS _{2/3} Se _{4/3}	222.7	481.4	288.9
MoS _{1/2} Se _{3/2}	230.5	465.1	303.6